UNIVERSITÀ DEGLI STUDI DI MILANO

DOTTORATO IN RICERCA BIOMEDICA INTEGRATA

XIX CICLO DI DOTTORATO

CARDIOVASCULAR COMPUTED TOMOGRAPHY AND MAGNETIC RESONANCE IMAGING IN CONGENITAL HEART DISEASE

Responsabile Dottorato: Chiar.ma Prof.ssa Chiarella SFORZA

Tutor: Chiar.mo Prof. Francesco SARDANELLI

Tesi di Dottorato

Dr. Francesco SECCHI

Matricola: R10682

ANNO ACCADEMICO 2015-2016

ABSTRACT

Cardiac magnetic resonance (CMR) is a non-invasive imaging modality highly reliable for studying cardiovascular morphology and function. Cardiac computed tomography (CCT) can give valuable anatomic information on CHD in children but implies radiation exposure, a relevant issue in children and newborns who are more radiosensitive than adult patients and have a longer lifetime to develop stochastic effects from radiation. We contributed to show the possibility to obtain an impressively low ionizing dose reduction in CHD patients also using standard 64-slice CT scanners. Conversely, CMR holds a pivotal role when functional and flow imaging is required. We showed the role of CMR in evaluating of patients percutaneously implanted with a pulmonary valve. Moreover, we proposed two new approaches for post-processing CMR images, regarding volume estimation of patients with a single ventricle, a rare CHD and a method for quantifying the paradoxical septal motion. CMR and CCT are two fundamental imaging techniques to evaluate patients with complex CHD. Both imaging modalities have limitations and advantages. CMR can evaluate heart function vessel flow but require a long acquisition time and in same patients a long sedation time. CCT has a very high spatial resolution and short acquisition time but implies ionizing radiation exposure. On the one side, we confirming the crucial role of CMR when function analysis is required but also showed the relevant possibilities of x-ray dose reduction in CCT, also using standard 64-slice scanners in the study of CHD patients.

INDEX

1. Introduction

1.1 Computed tomography: general overview

Multislice computed tomography (CT) allows for obtaining important information about anatomical and functional conditions of the heart during a single examination session. Cardiac CT (CCT) images in the context of non-cardiac-targeted thoracic studies are degraded by motion artifacts due to cardiac pulsation. In fact, routine thoracic CT studies that are not synchronized to the patient's ECG cycle. The synchronization of CT acquisition with the ECG allows obtaining images substantially free of motion artifacts. Non-contrast CCT scans synchronized to ECG for the end-diastolic phase allows the evaluation of calcium deposits in coronary atherosclerotic lesions. Notably, the CCT spatial resolution is higher than that of cardiac magnetic resonance (CMR), while CCT time resolution is lower than that of CMR. When a clinical balance between CCT and CMR has to be carried out, the ionizing radiation exposure of patients, in particular those in pediatric age, is an important issue to be considered. However, the recently reduction of ionizing radiation exposure with the last generation CT scanners opened a new scenario.

1.2 Cardiac magnetic resonance: general overview

CMR imaging is a technique highly reliable in evaluating the heart and related structures. It has a wide range of clinical applications: cardiomyopathies, coronary artery disease, heart failure, valvulopathies, congenital heart disease, and other non-ischemic alterations, such as primary cardiac tumors, cardiac metastases, and pericardial disease. Images of the heart are obtained along the most useful planes: the short axis, the horizontal long axis (also known as 4-chamber view of the heart), and the vertical long axis. Different sequences allow the physician to focus on different features of the heart, evaluating cardiac morphology and/or function. *Bright-blood* images, where the flowing blood signal is high, are mainly used to evaluate

function, whereas the *black-blood* images, where the flowing blood signal is suppressed, are mainly used to assess heart morphology. To evaluate acute and chronic myocardial dysfunction, late gadolinium enhancement sequences allow the physician to identify and quantify focal fibrosis caused by ischemic heart disease, such as myocardial infarction, or by other non-ischemic conditions.

CMR is crucial for the evaluation of congenital heart diseases (CHD), defined as defects of the cardiac structure present at birth. In CHD, genetic and/or environmental causes may impair the heart's development, and therefore its capability to properly provide deoxygenated blood to the lungs in the pulmonary artery, to receive oxygenated blood from the pulmonary veins, and to provide oxygenated blood to the aorta. CHD patients may also require much more frequent examinations than the general population from a very young age; an unregulated usage of CCT to evaluate their condition could have a great impact in terms of lifetime risk of cancer, as it will be addressed below. CMR provides a completely radiation-free tool, allowing physicians to obtain information as regularly as they may deem useful, without having to worry about the risk of significantly increasing the likelihood of cancer in these patients. However, especially in very young pediatric patients, a risk associated with a prolonged sedation, sometimes necessary for performing CMR, should be considered.

1.3 Cardiovascular imaging with CCT and CMR in CHD

Incidence of CHD is 4 -14 per 1000 live births, the isolated ventricular septal defect being the most common [1,2]. Other simple CHD are patent ductus arteriosus, atrial septal defect of the fossa ovalis (ostium secundum), isolated partial anomalous pulmonary venous connection, aortic coarctation, and bicuspid aortic valve [3]. The main complex CHDs are Fallot tetralogy (incidence 0.4 per 1000 live births), transposition of great arteries, double-outlet right ventricle, truncus arteriosus, and single ventricle [4]. Echocardiography is the first approach for CHD.

However, it is limited by operator dependence, acoustic window restrictions, and inability to detect extracardiac abnormalities [5]. Catheterization for digital subtraction angiography (DSA) is the reference procedure for treatment planning [6]. Cardiac magnetic resonance (CMR) is a non-invasive imaging modality highly reliable for studying cardiovascular morphology and function. However, it is limited in children by long scan times, requirement for sedation and close monitoring [7]. CCT can give valuable anatomic information on CHD in children but implies radiation exposure, a relevant issue in children and newborns who are more radiosensitive than adult patients and have a longer lifetime to develop stochastic effects from radiation [8]. However, newer CCT technologies allow for an optimized combination of highly reduced radiation exposure, high spatial resolution, and very short examination time [9], making CT for CHD competitive with CMR. Papers regarding x-ray dose reduction in CCT as well as CCT and CMR in CHD are shown in the following pages.

2. Paper on cardiac computed tomography

2.1 The feasibility of low radiation dose acquisition in pediatric patient using a 64-slice CT scanner (Under revision)

Purpose

The aim of this study was to evaluate the radiation dose and the image quality in pediatric cardiac CT angiography using a “standard” 64 slice scanner.

Materials and Methods

After institutional review board approval waived specific patient consent for data analysis, we retrospectively evaluated cardiac CT examinations performed in patients <18 years of age between the January 2010 and December 2014. CT examinations were performed on a 64-slice CT scanner (Somatom 64, Siemens Healthcare, Forchheim, Germany). Patients less than 3 years old need sedation. A dedicated protocol was performed according to the clinical issue. In the majority of patients non-contrast scan was waived to reduce radiation dose. A bolus of contrast agent from 5 to 60 mL (Iopamiro, Bracco) and saline water from 10 to 60 mL was injected intravenously at a flow rate from 1.5 to 3.0 ml/s according to patients characteristics. A test bolus injection technique was used. A time–enhancement curve was obtained by measuring the enhancement within the region of interest (ROI). The contrast agent arrival time was determined from the time to peak enhancement and was used to estimate scan delays for full-bolus diagnostic CT. This technique was used to study cardiac anatomy or coronary arteries. To acquire an angiogram we used the technique of bolus tracking, based on real-time monitoring of the main bolus during injection with the acquisition of a series of dynamic low-dose monitoring scans at the level of the vessel of interest. The trigger threshold inside the ROI was set at 100 HU above the baseline. The delay between each monitoring scan acquisition was 1.25 seconds. As soon as the threshold was reached,

the table moved to the cranial start position. During this interval the contrast material concentration increased to the desired level of enhancement. CT were performed using retrospective ECG-gating, prospective ECG-triggering, depending on the patient heart rate and rhythm and whether or not an evaluation of myocardial function was indicated or without ECG-gating. The reconstruction parameters were set as follows: the section thickness was 0.75 mm, reconstruction interval 0.45 mm, matrix size 512 × 512, field of view (FOV) 250 mm. Those two-dimensional (2D) imaging sequences were then transferred to another computer for 3D anatomy reconstruction. In our department we adopted the policy that pediatric CT studies were to be performed under the supervision of a cardiovascular radiologist and instructed technicians to minimize technical errors.

Estimation and Calculation of Effective Radiation Dose

The volume computed tomography dose index (CTDIvol) was automatically provided by the system and tube current and dose length product (DLP) were retrieved for each patient. Effective radiation dose (ED) in millisieverts (mSv) was calculated as DLP*k (mSv/mGy/cm) for chest. The conversion factor, k, varied with age and was estimated from the International Commission on Radiological Protection (ICRP) publication 103 recommendation [46]. ED was then evaluated per patient age group (0–6 vs. 6–12 vs. 12–18 years), and tube potential (kV) used.

Image Analysis

For assessment of image contrast signal-to-noise ratio (SNR) and contrast-to-noise ratio (CNR) were calculated for each scan using the following formulas:

$$SNR = HU_{left\ ventricle} / SD_{air}$$

$$CNR = [(HU_{left\ ventricle} - HU_{myocardium}) / SD_{air}]$$

Assessment of subjective image quality was performed by 2 observers. Image analysis was

performed individually, and image series were evaluated in random order.

Scans were classified using a Linkert scale in which a score of 3 was as very good, 2 was good, and 1 was poor or with significant artifact as per clinical practice at our institution.

Statistical Analysis. Statistical analysis was performed using statistical software (MedCalc version 12.7.2; MedCalc Software, Ostend, Belgium; Stata version 13; StataCorp, College Station, TX). Parametric variables are expressed in terms of mean and standard deviation (SD), whereas nonparametric variables are expressed as median and interquartile ranges (IQRs). Comparison of the median ED between two groups was performed using Mann–Whitney-U test, and between three or more groups using Kruskal–Wallis test. A p-value of <0.05 was considered significant.

For the qualitative image assessment the inter-observer agreement was evaluated using Cohen's kappa (κ) interpreted as follows: $\kappa < 0.20$ = slight agreement, κ: 0.21 – 0.40 = fair agreement, κ: 0.41 – 0.60 = moderate agreement, κ: 0.61 – 0.80 = substantial agreement, κ: 0.81 – 1.0 = almost perfect agreement.

Results

Study population

The study population included 47 patients (27 male, 20 female) with a mean of 7.6 ±5.5, years old. The most common primary indications for the CT examinations were aortic pathologies (n=15) and complex congenital heart diseases (n=13).

Spectrum of Radiation dose used

The median age-specific ED in our study population was 2.2 mSv (range: 0.1–12.1 mSv). Patients scanned using a tube potential of 80 kV had a significantly lower median radiation dose (0.2 mSV; range 0.1-0.2 mSv) compared to patients who were scanned using a tube potential of 100 or 120 kV , $p<0.001$. The subjective image quality was reported on all clinical

CT reports. Overall, 25 (53 %) scans were reported as ‘‘very good’’, 21 (45 %) as ‘‘good,’’ and 1 (2 %) as having significant artifact. The agreement between the two different readers was substantial k= 0,88.

In terms of objective image quality the mean SNR was 32.9, 30.2 and 28.3 at 120, 100 and 80 kV respectively and there were not significant using the different kilovoltage (p=0.90).

The mean CNR was 25.3, 19.4 and 20.3 at 120, 100 and 80 kV respectively (p=1.0).

There were not significant differences according SNR and CNR in the different age-group patients. In particular the mean SNR was 45.4, 36.3 and 29.4 in 0–6, 6–12 and 12–18 age group respectively (p=0.664). The mean CNR was 27.7, 25.4 and 20.1 in 0–6, 6–12 and 12–18 age group respectively (p=0.573)

Discussion

In this study we analyzed the assessment of cardiovascular CT in terms of radiation dose using a 64 slices scan in pediatric population with CHD. We demonstrated that using a dose-saving protocol the overall (not-ECG gated and ECG gated CT) median dose is 2.2 mSv. Our results are in line with other studies in the literature: the dose founded in some studies was 6.8 mSv [10] or 12 mSv [11] using a 64 slices scan and a retrospective gating.

In the more recent literature the advent of new generation scanners is related with a drastic decrease of radiation dose in pediatric setting. Han et al [12] analyzed a cohort of 70 pediatric patients and found an average ED of 1.7 mSv for retrospectively ECG-gated CT and 0.9 mSv for prospectively ECG-triggered CT. These findings highlighted the increasing role of CT in the pediatric setting with CHD and put this technique as an important tool to try to avoid diagnostic angiography. In fact, it was demonstrated that in a population of neonates with complex CHD referred for diagnostic cardiac catheterization after initial assessment by echocardiography and CT none required additional imaging. This is a goal in terms of reduction of radiation dose considering the median of 13.4 mSv occurs for diagnostic

catheterization.

Our study demonstrated that with a “standard” 64 slice scanner is possible to obtain good and diagnostic images. That is an important finding considering that the 64 slices remain the more diffused scanner. According to Italian registry of Cardiac Computed Tomography the 73% of scanner on national territory is a 64 slices [13]. In this scenario the impact of a dose saving protocol could be representing an important tool for the management of pediatric patient for the radiologist that works with a 64 slices scan.

Our experience suggests, since no differences were found in terms of SNR and CNR between the different kilovoltage setting used (120,100 and 80 kV) that an 80 kV protocol is adequate to image most pediatric patients. Also the agreement between the two different observers involved in our studies is not conditioned by the kilovoltage used.

The results of this study should be interpreted in view of its limitations. First then the number of patients is rather small and second because of the retrospective nature of the study.

In conclusion, CT is a valuable imaging modality when evaluating pediatric patients with a large spectrum of known or suspected cardiovascular abnormalities. Using dose-saving techniques, CT protocols tailored to the pediatric population and growing expertise, a cardiovascular CT in children with a low radiation dose using a 64 slices scanner is now allowed routinely.

3. Papers on cardiac magnetic resonance imaging

3.1. Cardiac magnetic resonance before and after percutaneous pulmonary valve implantation (Radiol Med 2014)

Purpose

To measure the magnetic resonance (MR) artefact produced by a percutaneous pulmonary valve stent and to evaluate the changes in volumetric and functional right ventricle (RV) parameters due to percutaneous pulmonary valve implantation (PPVI).

Materials and Methods

Preliminary in-vitro study

We studied a Melody ® valve measuring height of 24 mm and diameter of 22 mm inserted in a plastic box filled with echographic gel with common clinical cardiac sequences. The valve was oriented parallel to the main magnetic field in order to simulate the in-vivo orientation. Two readers (R1, R2), each of them with two years of experience in CMR, measured the size of signal void produced by the device artifact. Each of the two readers measured 16 values of diameter and 11 values of height. Mean, standard deviation, coefficient of variation (COV), and the difference between the size of signal void and the real valve dimensions were calculated.

Study design and population

After Institutional Review Board approval, we retrospectively analyzed our reports of pre-/post-PPVI CMR studies performed from January 2008 to June 2010 in 27 consecutive patients (12 females, 15 males), aged 22±9 years (mean±standard deviation) treated with PPVI. CMR was performed at least one month before PPVI, and one, three, and six months after PPVI. All 27 patients underwent CMR before PPVI while not all patients performed all the three CMRs after PPVI: 13/27 patients were studied after one month, 20/27 after three

months, and 21/27 after six months.

CMR protocol

We used a 1.5-T unit with 40-mT/m gradient power (Magnetom Sonata Maestro Class, Siemens, Erlangen, Germany) and a four-channel cardio-thoracic coil. The same protocol was used before and after PPVI. Electrocardiographically (ECG)-triggered short-axis, four chamber, and long-axis images were obtained with a steady-state free precession sequence (true fast imaging with steady-state free precession, true-FISP) acquired with the following technical parameters: TR/TE=4/1.5 ms, FA=80°, thickness 7 mm and temporal resolution 45 ms. A free-breathing turbo spoiled gradient echo sequence (fast low angle shot, FLASH) was performed for phase-velocity mapping of pulmonary flow with following technical parameters: TR/TE=4/3.2 ms, thickness 5 mm, velocity encoding from 150 to 350 ms, and temporal resolution 41 ms. Before PPVI the slice was located in the pulmonary conduit, perpendicular to the long vessel axis, immediately distal to the valve; after PPVI, the slice was located 4 mm distal to the stent artifact.

Image analysis

Cine true-FISP images on short axis plane, from hear base to the apex, were segmented semi-automatically (Syngo-Argus, version VE32B, Siemens Medical Solutions, Erlangen, Germany) by a reader with 6 years of experience in CMR imaging, to obtain ejection fraction (EF), end-diastolic volume (EDV) normalized to body surface area (EDV index, EDVI), and end-systolic volume index (ESVI) of RV and left ventricle (LV). Papillary masses were excluded from volume. Reverse flow, forward flow and peak velocity data of pulmonary valve were obtained segmenting phase-contrast flow images with the same software. We estimated pulmonary RF by flow data. Pressure gradient was estimated from peak flow velocities using Bernoulli's equation.

Catheterization and echocardiography

The peak-to-peak RV- PA gradient was calculated during this procedure as the difference in systolic pressure between RV outflow tract and main PA distal to the conduit before the implanting valve procedure. Before and three month after PPVI conduit mean pulmonary PG was calculated on echocardiography by tracing the border of continuous-wave spectral Doppler recordings and integrating the area under the curve. Maximum instantaneous PG was also estimated by echocardiography.

Statistical analysis

Differences between the two readers of the in-vitro study were tested with the Wilcoxon test. Wilcoxon test was also used to compare EDVI, ESVI, EF, RF and PG before and after PPVI. All testing was performed using SPSS statistical software for Windows, release 14.0 (SPSS Inc., Chicago, IL, USA). Values of $p<0.05$ were considered significant.

Results

Preliminary in-vitro study

For R1 the mean diameter was 21.9±1.0 mm (COV=4.6%) and mean height was 25.0±0.8 mm (COV=3.4%); for R2 the mean diameter was 22.1±1.3 (5.8%) and mean height was 25.1±1.1 (4.5%). Pooling the data, the number of cases with an absolute measured-to-actual difference >1.5 mm was 5/27 (4/5 differences ≤2 mm) for both readers. The difference between the two readers was not significant for both the diameter (p=0.844) and the height (p=0.503).

In-vivo study

All CMR data and comparisons are showed in Table 1.

Table 1

CMR data before and 1, 3, and 6 months after percutaneous pulmonary valve implantation

	13 Patients			20 Patients			21 Patients		
	pre PPVI	1 month	P	pre PPVI	3 months	P	pre PPVI	6 months	P
RV EDVI									
(mL/m^2)	71±20	70±23	0.506	83±42	66±22	0.013	79±42	64±21	0.050
RV ESVI									
(mL/m^2)	36±19	33±16	0.195	46±42	32±16	0.002	43±41	30±14	0.021
RV EF (%)	50±10	55±13	0.065	47±14	53±14	0.031	49±13	54±12	0.018
LV EDVI									
(mL/m^2)	65±18	69±20	0.410	65±12	73±18	0.059	64±15	73±21	0.034
LV ESVI									
(mL/m^2)	30±11	31±10	0.916	31±9	31±9	0.613	30±9	33±4	0.508
LV EF (%)	54.9±7	55.9±9	0.609	54±7	57±7	0.107	54±7	57±10	0.147
RF (%)	15±19	1±3	0.025	12±13	2±4	0.01	14±18	2±5	0.013
PG (mmHg)	34±18	11±10	0.003	31±19	15±15	0.001	36±15	13±15	<.001

PPVI: percutaneous pulmonary valve replacement. RV: right ventricle. LV: left ventricle. EDVI: end-diastolic volume index. ESVI: end-systolic volume index. EF: ejection fraction. RF: regurgitation fraction. PG: pressure gradient. Data are presented as mean±SD.

Considering 21 patients data before and 6 months after procedure, EDVI, ESVI and EF of RV before PPVI was 79±42 mL/m2, 43±41 mL/m2 and 49±13 % respectively; after PPVI was 64±21 mL/m2 (p=0.054), 30±14 mL/m2 (p=0.021) and 54±12 % respectively (p=0.018). No significant differences were found in terms of LV ESVI and ejection fraction. We found a significant difference between EDVI before (64±15 mL/m2) and after (73±21 mL/m2) PPVI (p=0.034). Pressure gradient and RF before PPVI were 36±15 mmHg and 14±18 % respectively and after PPVI 13±15 mmHg (p<0.001) and 2±5 % (p=0.013).

Before PPVI the mean gradient and the maximum instantaneous PG measured by

echocardiography were 38±7 mmHg and 76±14 mmHg respectively. The same data 3 months after PPVI were 16±9 mmHg and 27±15 mmHg respectively. Peak RV-to-PA gradient measured by catheter before PPVI was 41±17 mmHg. No significant differences were found comparing CMR PG, echocardiography mean PG (p=0.382) and catheter PG (p=0.586). Significant difference was found between echocardiography maximum instantaneous PG and CMR before (p=0.001) and after PPVI (p=0.010).

Figure 1 shows LV EF, RV EF, RF and PG evolution before/after PPVI.

Fig 1

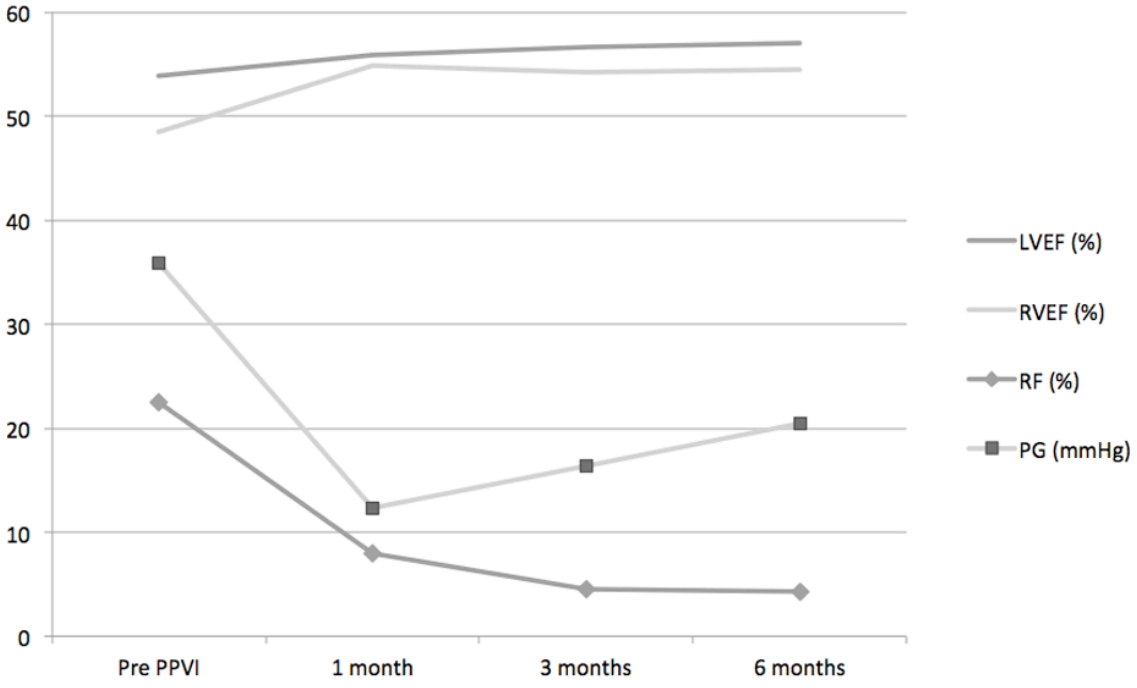

Discussion

In patients with congenital heart disease, usually treated with many surgical procedures, to use a low-invasive procedure to treat the pulmonary valve or conduit dysfunction, such as PPVI, is a relevant clinical issue. This in-vitro/in-vivo study showed that: 1) the artifact from MR sequences is sufficiently small for not influencing qualitative and quantitative MR

evaluation after PPVI; 2) there is a significant reduction of PG and RF and a significant increasing of RV function.

The low interobserver variability of the artifact size (COV 3.4-4.6%) showed the reliability of our measurements. Looking at the artifact size, we showed that SSFP, half-fourier acquisition single-shot turbo spin-echo (HASTE), and turbo spin-echo (TSE) sequences produced the most accurate valve measurement, i.e. less than 1.5 mm in the difference between the MR measures and the real size of the valve. This means that these MR sequences are suitable for clinical evaluation of the heart with Melody® valve as previously demonstrated for different type of vessel stents in an in vitro model [14].

In the in-vivo study, we evaluated the pre-treatment and follow-up CMR study of patients treated with a PPVI. One month after PPVI we found a significant reduction of pulmonary PG and RF but no significant changes of RV volumes and EF. The most probable reason is that the hemodynamic effect of PPVI needs more time than one month to be effective in terms of chamber volumes and pump function. In fact, both 3 months and 6 months after PPVI, we found a significant reduction of both diastolic and systolic RV volumes and a significantly increased RV EF, accordingly to literature data [15-18]. Regurgitation fraction was significantly reduced since the first control one month after PPVI and even PG decreased significantly, showing a good performance of the Melody® valve.

Up to now, we found only a significant increase of EDVI for LV at 6 months after PPVI. No other significant differences were found for LV. This result plays in favor of a possible positive PPVI effect on LV function but further long-term studies are needed to confirm this hypothesis.

RV EDVI and ESVI decreased during time and the RV EF reached a plateau. Conversely, a significant increase at this time of the LV EDVI produced a small but not significant increase of LV EF. Regurgitation fraction and PG remained below the clinical relevance after an

evident and significant drop down.

Before PPVI, we did not found any significant difference between catheter and CMR PG values. However, when we use the catheter peak-to-peak PG as a reference standard for PG measured by CMR or echocardiography, we should consider that PG is calculated through the peak velocity both in echocardiography and CMR while catheter peak-to-peak PG is calculated as the difference between the maximal pressure in PA and in the RV which happen in two different time of the cardiac circle. Thus, catheter peak-to-peak PG could be inappropriate as a reference standard. Moreover, comparing the echocardiography maximum instantaneous PG to the CMR PG, we found a significant difference but no differences if comparing CMR PG to the echocardiography mean PG. Therefore, it could be better to consider comparable the catheter peak-to-peak PG, the echocardiography mean PG and CMR PG. This could be a finding, which deserve further investigation.

This study has some limitations. First, we studied a heterogeneous population with different congenital hear diseases traded with different surgical approaches. However all patients present the same condition of pulmonary stenosis/insufficiency treated with PPVI. Second, not all 27 patients performed completely a 3-step follow-up. However, the evaluation of patients for each follow-up step clearly showed the hemodynamic PPVI effect. Third, we did not estimate the inter- and intra-observer reproducibility of in-vivo CMR. However, CMR is commonly considered more reproducible than echocardiography in the evaluation of the right chambers, RVOT and pulmonary artery [19]. The last limitation of this study in that there is no a comparison with different pulmonary valve stent.

In conclusion, the signal void produced in vitro by the metallic structure of Melody® pulmonary valve is limited to its inner space with a maximal extent to the external space equal to less than 5 mm. Moreover, CMR evaluation of patients after 6 months from PPVI shows a drastic decrease of RF and PG and a significant improvement of all RV parameters. CMR can be

used for a comprehensive noninvasive assessment of cardiac performance after PPVI. The long-term performance of Melody® pulmonary valve and its effect on the LV function remain to be investigated in further larger studies.

3.2 Segmentation of cardiac magnetic resonance cine images of single ventricle: including or excluding the accessorial ventricle? (Int J Cardiovasc Imaging 2014)

Purpose

Our aim was to compare two different approaches for segmentation of single ventricle (SV) on cardiac magnetic resonance (CMR) cine images.

Materials and Methods

Study Design and Population

We retrospectively studied 30 patients (23 males and 7 females; aged 27±10 years) with diagnosis of SV malformation treated with systemic-pulmonary shunt or Fontan procedure. Thirteen of these 30 patients had an anatomic SV, while 17 a functional SV. In particular, the diagnosis before surgical intervention was: pure SV (n=13), tricuspid atresia (n=8), pulmonary atresia (n=5), mitral atresia (n=2), pulmonary stenosis with right ventricle hypoplasia (n=2).

CMR Protocol

We used a 1.5-T unit with 40-mT/m gradient power (Magnetom Sonata Maestro Class, Siemens Medical Solutions, Erlangen, Germany) and a four-channel cardio-thoracic phased-array surface coil. Electrocardiographically-triggered steady-state free precession axial sequences (true fast imaging with steady-state free precession, FISP) were acquired with the following parameters: time of repetition (TR) ~ 4.3 ms, depending on the R-R interval of the cardiac cycle; time to echo (TE) 2.2 ms; flip angle (FA) 74°; 2 excitations; slice thickness 5 mm; 40 no-gap slices; pixel size 1.4 mm × 1.4 mm; acquisition time 50 s. Half-Fourier single shot turbo spin-echo (HASTE) three-plane sequences were also acquired with the following parameters: TR~800 ms; TE 25 ms; FA=160°; slice thickness 6 mm. Cine short-axis, four chamber, and long-axis images were obtained with true-FISP sequences acquired with the following parameters: TR ~ 4 ms; TE=1.5 ms; FA=80°; thickness 8 mm; temporal resolution 45

ms. According to the clinical indications, flow sequences and/or MR-angiography were also performed.

Image analysis

We classified patients as having one or more of the following characteristics:

- Visceroatrial situs: solitus (S), inversus (I), or ambiguous (A)
- Orientation of cardiac axis: dextrocardia, or levocardia, or mesocardia
- Ventricular loop: dextro (D)- or levo (L)-ventricle loop
- Right or left morphology of the SV
- Position of great arteries (GA): normal position (S) with aorta posteriorly and rightward to the pulmonary artery; inverted position (I) with aorta posteriorly but leftward to the pulmonary artery; D- or L-transposition (TGA) with aorta anteriorly to pulmonary artery and rightward or leftward respectively; or D- or L-malposition (MGA) when aorta is neither anterior nor posterior to pulmonary artery.

Cine true-FISP images in short-axis plane were segmented semi-automatically (Syngo-Argus, v. VE32B, Siemens Medical Solutions, Erlangen, Germany) by a reader with 5 years of experience in CMR imaging. Ejection fraction (EF), indexed end-diastolic volume (EDVI), end-systolic volume (ESVI) and stroke volume (SVI). Volume analysis was performed twice, firstly including only the systemic ventricle, secondly including both systemic and accessorial ventricles, blinding the reader to results of measurement of the first approach.

Statistical Analysis

Signed rank Wilcoxon test was used to compare EF, EDVI, ESVI and SVI obtained using the two different volume analyses. All calculations were performed using SPSS Statistics v. 19 (SPSS, Chicago, IL) and Excel (Microsoft Excel® 2010, Redmond, WA). A p-value less than 0.05 was considered as significant.

Results

All patients were treated with the Fontan procedure, 12 with classic Fontan. Twenty-seven patients were found with situs solitus, 2 patients with situs ambiguus with asplenia and 1 situs ambiguus with polisplenia. Twenty-five patients had levocardia, 4 patients dextrocardia and 1 mesocardia. Twenty-seven patients had D-ventricle loop and 3 L-ventricle loop. Four patients showed right morphology of the SV. We found 13 L-TGA, 4 L-MGA, 4 D-MGA, 3 D-TGA and 1 inverted vessel position. At the volume analysis we excluded 3 patients due to a poor quality of the cine-MR images. Thus, 27 patients were analyzed. When segmenting both systemic and accessorial ventricles (Fig 2), EDVI and ESVI were significantly higher than those obtained segmenting only the systemic ventricle (Fig 2) while no significant difference was observed for the SVI. The EF obtained segmenting both systemic and accessorial ventricles resulted significantly lower than that obtained segmenting only the systemic ventricle.

Fig. 2

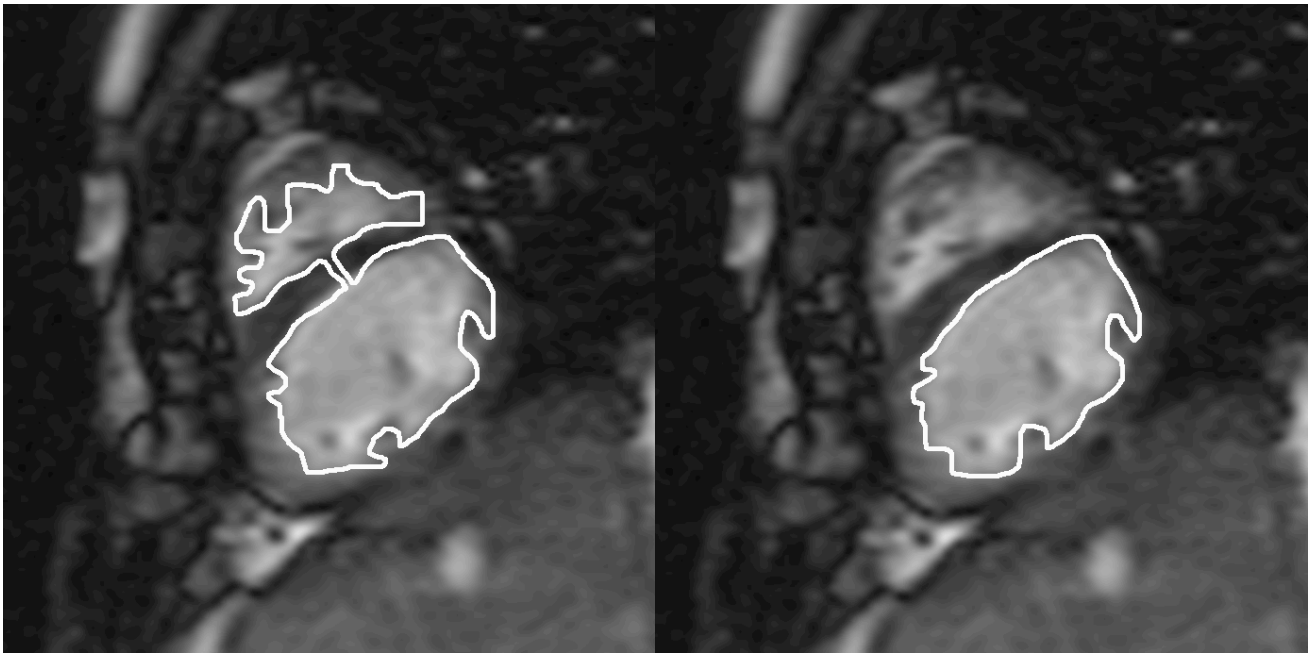

Discussion

Advances in pediatric cardiac care resulted in a population of adults with CHD being followed up in tertiary care centers, a part of whom undergoing a palliative or reparative surgery during their early life [20]. As reported by several studies [21, 22], we will face more and more with adults than with children affected with CHD, due to better diagnostic and therapeutic capabilities. Lifelong follow-up is required to optimize quality and span of life. Cardiac magnetic resonance plays a key role for CHD patients and has become routine practice during the last decade [21, 23]. Other than detailed anatomic views, CMR enables a functional assessment of ventricles, valves, and shunts, both qualitatively and quantitatively [23], sparing the patients with the ionizing radiation associated to computed tomography. Moreover, CMR in CHD patients usually does not require intravenous administration of contrast material (although contrast material can be safely used, if necessary) [21]. In this study, we analyzed the results of CMR performed in 30 patients with SV malformation treated with Fontan procedure. Anatomical analysis was successful in all patients, including the 3 subjects with low quality of cine MR images that impaired the functional analysis. Regarding volume analysis, we used two different approaches: (1) including only the systemic ventricle; (2) including both systemic

and accessorial ventricles. As expected, adding the accessorial ventricle to the systemic ventricle in the segmentation process, a significant increase in both EDVI (8 mL/m^2, 19%) and ESVI (7 mL/m^2, 25%) was observed, associated to an unchanged SVI (the difference was only 1 mL/m^2). Vice versa, the median EF was significantly lower (from 49% to 44%), allowing for speculating that the contribution of the accessorial ventricle to the pump function is negligible. Moreover, our result on the EF also implies that the longitudinal evaluation of these patients with CMR should be performed using always the same approach. In our opinion, due to the negligible absolute contribution to the SVI, we recommend that the accessorial ventricle should be ignored. Even in healthy subjects and Fallot patients a significant regional differences between the sinus and infundibulum components of the RV were demonstrated [24,25,26]. An important consideration, regarding our population, is that we pooled patients with “anatomic’’ single ventricle and ‘‘functional” single ventricle. In the first case there is an accessorial chamber and in the second a RV connected to the LV with a big interventricular septal defect. However, in both conditions there is only the systemic connection to the aorta without pulmonary connection; thus, we can consider these two groups of patients homogenous. Soriano and coauthors [27] studied a sample of young patients with SV (mean age 7 months), comparing three-dimensional echocardiography measurements of SV volume, mass and EF with those measured by CMR. Their segmentation methods of CMR images were not completely described but the accessorial ventricle was not specifically mentioned [26]. Our study has limitations. Firstly, this is a retrospective study on a relatively small number of subjects, based on a single-center historical series of SV patients. However, this was a consecutive series of a relatively rare disease. Second, only one reader examined CMR images and we did not estimate intra-observer reproducibility of volume measurement (the evaluation was performed by the most experienced radiologist routinely dedicated to cardiac imaging).

In conclusion, CMR is an optimal technique to define the correct cardiac anatomy and function of SV patients. Our findings support the hypothesis that the accessorial ventricle does not contribute to the pump function. Physicians should be aware that the inclusion of the accessorial ventricle in the segmentation post-processing may lower the EF.

3.3 A geometric index to differentiate abnormal from normal septal wall motion on cardiac MR imaging (Acta Radiol 2015)

Purpose: The definition of abnormal septal wall motion (SWM) is usually performed on a subjective visual assessment with cardiac MR (CMR).

Material and Methods

Population

Local Ethics Committee approval was obtained for this retrospective study, including a consecutive series of 100 patients who underwent CMR examination at our institution from September 2009 to March 2010. They were 73 males and 27 females (mean age±standard deviation 43±22 years).

CMR Imaging Protocol

All examinations were performed with a 1.5-T MR unit with 40-mT/m gradient power (Magnetom Sonata Maestro Class, Siemens Medical Solution, Erlangen, Germany) and a 4-channel phased-array surface coil. Cardiac kinetics was evaluated on cine 4-chamber and short-axis planes obtained with unenhanced balanced steady-state free precession sequence acquired with the following technical parameters: time of repetition ~4.3 ms, depending on the R-R interval of the cardiac cycle, time of echo 1.5 ms, flip angle 80°, slice thickness 7 mm, retrospective ECG-trigger. Morphology was assessed with an ECG-triggered unenhanced balanced steady-state free precession sequence on axial plane with the following technical parameters: time of repetition ~4.3 ms, depending on the R-R interval of the cardiac cycle, time of echo 1.1 ms; acquisition time ~ 1 minute, field of view 275×400 mm^2, slice thickness 5 mm.

Image Analysis

All CMR examinations were independently reviewed by two readers with 4 (R1) and 2 (R2) years of experience in CMR. For each patient, R1 performed both qualitative and quantitative

analysis on mid-ventricular short-axis images. For qualitative analysis, R1 analyzed the septal convexity and subjectively defined whether an abnormal SWM was present at the end-systolic and/or end-diastolic phases on short axis images. For the quantitative analysis, R1 measured the septum curvature at least one week before or after the qualitative analysis, applying the following protocol (Fig. 3):

1. selection of the mid-ventricular slice on short axis slice;
2. measurement of the distance from anterior to posterior septal RV/LV junctions (defined as the connection between anterior or posterior RV and LV wall in the septum) applying a ruler perpendicular to the endocardial surface (segment **a** in Fig. 3);
3. measurement of the maximal distance from the endocardial septum surface perpendicularly to the segment **a** (segment **b** in Fig. 3);
4. calculation of the **b**/**a** ratio, that was used as a measure of the convexity septal index (CSI) of the interventricular septum.

Fig. 3

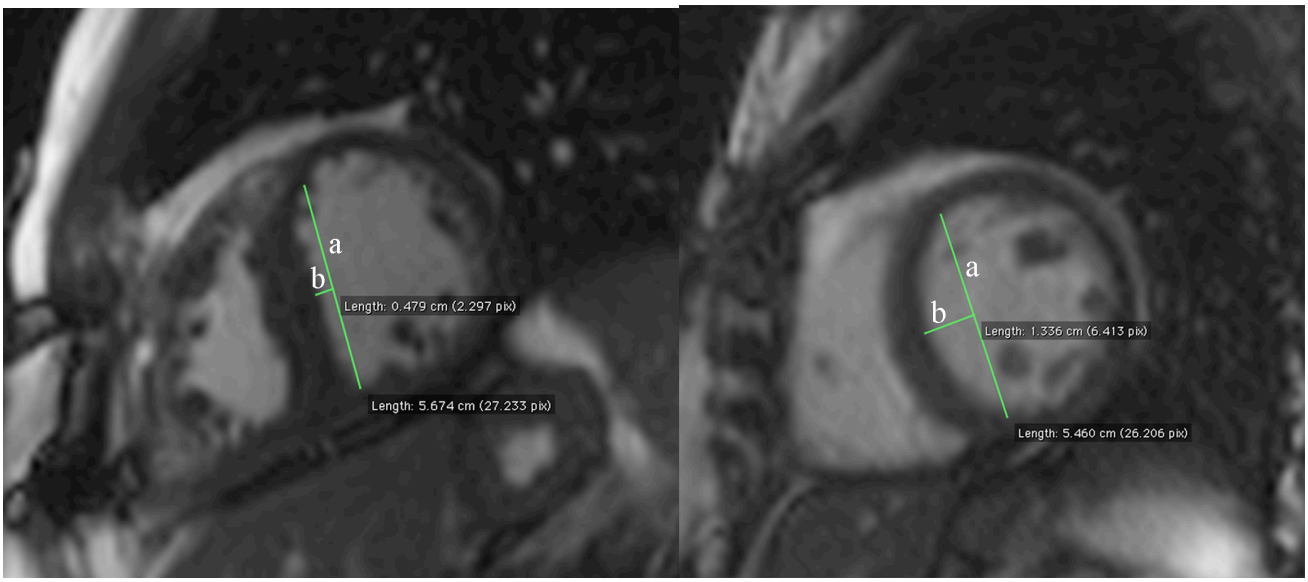

This measurement protocol was applied both in end-systolic and end-diastolic phases. The coronary sinus diameter was measured using axial ECG-triggered unenhanced balanced steady-state free precession sequence. Using the middle 4-chamber plane at end-systolic phase, the right atrium area was also measured. In order to estimate the inter-reader reproducibility, R2 repeated the qualitative and quantitative CSI diastolic evaluation.

Reference Standard and Statistical Analysis

Inter-reader reproducibility was estimated using Cohen κ statistics for qualitative analysis and Bland-Altman method for quantitative analysis. Referring to differences between the two datasets (R1 – R2) of quantitative analysis, the coefficient of repeatability (CoR) was calculated as:

$$\text{CoR}=1.96 \times \text{Standard Deviation (R1–R2)}$$

And reproducibility was calculated as:

$$\text{Reproducibility} = \left[1 - \frac{\text{CoR}}{\text{Mean(R1, R2)}}\right] \times 100$$

where Mean(R1,R2) is the grand mean calculated using values obtained by the two readers. Referring to the qualitative visual analysis, the study sample was retrospectively subdivided in three groups, as follows: group A, including patient with normal SWM; group B, including patients with abnormal SWM only at end-systolic phase; group C, including patients with abnormal SWM at both end-systolic and end-diastolic phases. The comparison of the median CSI among the three groups of patients was performed using the Kruskall-Wallis test, while the paired comparisons were performed using the Mann-Whitney *U* test. The CSI trend among the three groups was tested using the Jonckheere-Terpstra test. The same strategy was applied for the coronary sinus diameter and the right atrium area. We estimated the interstudy variability in a volunteer who repeated CMR nine times. To this end, R1 measured the septum

curvature at the same level in short axis images. Interstudy variability was expressed in terms of coefficient of variation, i.e. the ratio between the standard deviation and the mean of the nine measurements. The correlation among end-systolic CSI, coronary sinus diameter, and right atrium area was estimated using the Spearman correlation coefficient. This analysis has been repeated for end-diastolic CSI. Continuous variable were presented as median and interquartile interval. P-values lower than .05 were considered significant. All testing was performed using SPSS statistical software for Windows, release 17.0 (SPSS Inc., Chicago, IL).

Results

Out of 100 patients, 73 were diagnosed with a normal SWM at qualitative visual evaluation (group A). Of the remaining 27 patients, 9 showed an abnormal SWM at end-systolic phase (group B), and 18 at both end-systolic and end-diastolic phases (group C). Two patients had a negative CSI, associated with a paradoxical abnormal SWM. The time for the visual analysis was about 3 minutes, that for quantitative analysis about 4 minutes (including CSI calculation for both phases).

Inter-reader reproducibility and interstudy variability

Cohen κ coefficient for the inter-reader reproducibility of qualitative evaluation resulted to be almost perfect (k=0.841, p<0.001). Regarding quantitative analysis, CoR obtained using the Bland-Altman method was 0.05, corresponding to an inter-reader reproducibility of 77%. The coefficient of variation of the interstudy variability estimated on the volunteer was 15% in diastole and 9% in systole.

Convexity septal index in normal and abnormal subjects at visual evaluation

At end-systole, the median CSI was 0.23 for group A (normal subjects at visual evaluation), significantly higher than that (0.13) of group B (abnormal SWM at visual evaluation only at end-systole), and that (0.10) of group C (abnormal SWM at visual evaluation at both end-systole and end-diastole). Similarly at end-diastole, when the median CSI was 0.25, 0.15, and 0.12,

respectively. The CSI trend among the three groups was significant, at both phases. The median coronary sinus diameter of group A (8 mm) was significantly smaller (p=0.009) than that of group C (median 11 mm); although the trend for the coronary sinus diameter along the three groups was significant (p= 0.007), the comparisons between group A and group B and between group B and group C were not significant. The median right atrium area was not significantly different among the three groups of patients (p= 0.246).

Correlations

Coronary sinus diameter resulted positively correlated with right atrium area (r = 0.332, P= 0.001). At bivariate analysis, while end-systole CSI negatively correlated with both right atrium area (r = -0.197, p= 0.049) and coronary sinus diameter (r = -0.245, p= 0.015), end-diastole CSI showed a trend towards significance or a borderline P value for negative correlation with right atrium area (r = -0.164, p= 0.104) and coronary sinus diameter (r = -0.193, p= 0.056).

Discussion

Abnormal SWM consists of the interventricular septum moving anteriorly during systole. It occurs when the heart center of gravity is shifted into the RV because of its volume and/or pressure overload [28]. Many conditions, congenital or not, may cause abnormal SWM. Examples include Fallot tetralogy, transposition of great arteries, congenital absence of pericardium, septal ischemia or infarction, left branch bundle block, constrictive pericarditis, and valve disease [29]. In clinical practice, the SWM can be evaluated with M-mode or color-tissue Doppler echocardiography [28]. Using color-tissue Doppler, the wall motion toward the probe is colored red, whereas the wall motion away from the probe is colored blue. In abnormal SWM, the point of the color change shifts towards the apex [29]. Another technique to assess SWM is the gated single-photon emission tomography with perfusion tracers using regional wall motion assessment [29]. However, echocardiography and single-photon emission computed tomography have suboptimal performance due to the possibility of poor acoustic

window and relatively low spatial resolution, respectively [28]. Several authors [30,31] reported on the use of CMR for this purpose. CMR with cine sequences is considered the most reliable technique for quantitative evaluation of cardiac function, outperforming other techniques in terms of reproducibility, without exposure to ionizing radiation. Systolic SWM reflects a condition of pulmonary stenosis or pulmonary hypertension; conversely diastolic SWM reflects a right ventricle volume overload. In this study, we defined a geometric index, the CSI, for measuring the septal convexity at CMR in order to distinguish normal from abnormal SWM. We tested CSI both in end-systolic and end-diastolic phases and evaluated its value in three different groups of patients on the basis of qualitative, visual global evaluation of SWM. The excellent inter-reader reproducibility ($\kappa = 0.841$) of this qualitative visual evaluation reinforced our use of their results for subdividing the patients in the groups. In this study, 27 of 100 patients showed abnormal SWM at visual evaluation. Almost half of them (n = 12, 44%) had a pulmonary valve stent implantation, this subgroup of patients having the highest prevalence (80%) of abnormal SWM, as expected. In fact, patients needing a pulmonary valve stent implantation are mainly those presenting with a valve regurgitation (associated or not associated with a valve stenosis). This condition may cause a RV pressure and/or volume overload and, as a consequence, an abnormal SWM, as demonstrated by Roeleveld et al. who showed a pulmonary arterial pressure higher than 67 mmHg in patients with abnormal SWM [32].

We found a significant difference in end-systole CSI between group A not only if compared with group C but also with group B. This result confirms that our geometrical approach works to quantify the SWM but does not seem to add “anything else” than quantification. Its mathematical definition determines the negative CSI value when the septum has a paradoxical bowing towards the left chamber, as we had in two patients. Obviously, when CSI is exactly equal to 0, the septum is perfectly flattened (one case, in systolic phase, in our series).

Interestingly, we found also for end-diastole CSI a significant difference not only between group A and group C, but also between group A and group B. This last result opens an intriguing window. In fact, end-diastole CSI seems to allow for detecting an abnormal SWM in patients with normal SWM at visual evaluation. We can speculate that this occurs because an abnormal SWM in systole could generate a minimal SWM alteration even in diastole that could be detected by quantification with CSI only. As a confirmation of this finding, no significant differences were found comparing group B and group C both at end-systole and end-diastole. Coronary sinus diameter was significantly smaller in group A than in group C and no significant differences were found between group A and group B for this variable. We can speculate that a volumetric and/or pressure RV overload, analyzed with visual assessment, produces an enlargement of coronary sinus. At correlation analysis involving CSI at end-systole, we found a significant negative association between CSI and the coronary sinus diameter and the right atrium area, separately. From these results, one may conclude that the lower the CSI (i.e., the more abnormal is SWM), the larger the right atrium area and the coronary sinus diameter. Thus, the right atrium area resulted associated to the coronary sinus diameter regardless the presence of an abnormal SWM. This is a consequence of a pressure overload in particular regarding our patient's sample (89% of patients with abnormal SWM had congenital heart diseases). At correlation analysis involving CSI at end-diastole, we found a negative correlation with a trend towards significance or borderline significance between CSI and right atrium area or coronary sinus diameter, probably due to a too small sample size. This is not the first approach to quantify SWM proposed in the literature. Using Doppler echocardiography Louie et al. [33] presented a geometric index to quantify the ventricular septal displacement in 11 patients who underwent tricuspid valvulectomy. This was a left ventricle eccentricity index of the short-axis profile, calculated at end-systole, mid-diastole, and end-diastole. A more recent study by Mori et al. [34] showed another left ventricle eccentricity index derived from the

ratio of two short-axis diameters measured at early diastole in 32 consecutive patients with pulmonary hypertension. Apart from the relatively small sample size of both studies including single disease and the use of echocardiography, these two indices have slight differences in-between them, both including the length between the septum and the left free wall. This implies a high dependence on what happens to the entire left ventricle than what happens to the septum. In fact, both of them were named “eccentricity” indices while what we are presenting here is a “convexity septal index”. In 2005, Roeveled et al. [32] proposed an interesting method to evaluate the septum curvature and correlate it with systolic pulmonary arterial pressure in patients with pulmonary hypertension using CMR. The septal curvature was measured in the short-axis image plane at the most basal level and was defined as the reciprocal of radius of curvature. However, the main aim of this method, based on an analytic calculation, was to predict whether in a specific population of patients with systolic pulmonary arterial pressure > 67 mm Hg there was a leftward septal curvature. The potential advantage of our CSI if compared with that method of evaluation of septal curvature is its simplicity and the short time needed to obtain it (only 4 minutes, compared to 3 minutes for visual evaluation).

Our study has three limitations. First, this is a retrospective study. The CSI should be prospectively tested in large consecutive series of patients with different cardiac diseases and clinical conditions. Second, the sample size was relatively small, even if composed by a consecutive series with a relatively high rate of abnormal SWM (27%) which allowed for a first demonstration of the method. Third, we did not estimate intra-observer reproducibility, which could be even better than the inter-observer reproducibility (77%), allowing for a highly reliable longitudinal evaluation of these patients by an individual reader.

In conclusion, this study supplies a proof of concept that end-systole and and-diastole CSI enable us to quantify SWM at CMR in a simple, easy, and reproducible way. Moreover, end-

diastole CSI seems to be sensitive in detecting an abnormal SWM in patients with apparently normal SWM at visual evaluation.

3.4. Four-year cardiac magnetic resonance (CMR) follow-up of patients treated with percutaneous pulmonary valve stent implantation (Eur Radiol 2015)

Purpose

To investigate follow-up after percutaneous pulmonary valve implantation (PPVI).

Materials and Methods

Study design and population

After institutional review board approval which waived specific patient consent for data analysis, we retrospectively retrieve prospective reports of CMR examinations performed before and after PPVI from January 2008 to June 2014 in 40 consecutive patients treated with a Melody valve stent (Medtronic, Inc., Minneapolis, MN, USA). CMR had been planned at least 1 month before PPVI, and 1, 3, 6, 12, 24, 36, and 48 months after PPVI. Pediatric cardiologists obtained informed consent for the intervention and use of this type of valve for PPVI. Informed consent was obtained by each patient for the injection of Gd-based contrast material, when administered.

CMR protocol

We used a 1.5-T unit with 40-mT/m gradient power (Magnetom Sonata Maestro Class, Siemens, Erlangen, Germany) and a four-channel cardio-thoracic phased-array coil. The same imaging protocol was used before and after PPVI. CMR mean duration was 45±10 min. Electrocardiographically-triggered short-axis, four-chamber and long-axis images were obtained with a breath-hold steady-state free precession (SSFP) sequence (true fast imaging with SSFP, true-FISP) acquired with the following technical parameters: TR/TE, 4.0/1.5 ms; FA, 80°; slice thickness, 7 mm; temporal resolution, 45 ms; mean acquisition time 14±4 s. A breath-hold turbo spoiled gradient echo sequence (fast low-angle shot, FLASH) was performed for phase-velocity mapping of pulmonary flow with the following technical parameters: TR/TE,

4.0/3.2 ms; slice thickness, 5 mm; velocity encoding (VENC) from 150 to 350 ms; temporal resolution, 41 ms; mean acquisition time 15±4 s. Firstly we acquired the phase-contrast sequence with a VENC of 150 ms; in the presence of aliasing, we modified the VENC adding 50 ms for each new sequence, step-by-step up to the complete disappearance of the aliasing artifact. Before PPVI, the slice of phase-contrast sequence was located in the pulmonary conduit, perpendicular to the vessel long axis, immediately distal to the valve; after PPVI, the slice was located at least 4 mm distal to the stent artifact to avoid contamination of images from the metallic artifact. Conventional angiography with a three-dimensional gradient-echo fast low-angle shot sequence (FLASH, TR=3.32 ms, TE=1.21 ms, flip angle 25°, slice thickness=1.5 mm, 72 partitions, acquisition time 21 s) after injection of 0.1 mmol/kg of gadobenate dimeglumine (MultiHance, Bracco Imaging SpA, Milan, Italy) was performed only at the baseline CMR before PPVI. MR angiography was not performed after PPVI due to the presence of metal artifact in the pulmonary conduit.

Image analysis

Cine true-FISP images in the short-axis plane, from heart base to apex, were segmented semiautomatically (Syngo-Argus, version VE32B, Siemens Medical Solutions, Erlangen, Germany) by a reader with 7 years of experience in CMR imaging, to obtain end-diastolic volume (EDV) normalized to body surface area (EDV index, EDVI), end-systolic volume index (ESVI), stroke volume (SVI), and ejection fraction (EF) of RV and left ventricle (LV). Papillary muscles were excluded from the volume. The basis was chosen with the references of 4-chamber view. Reverse flow, forward flow and peak velocity data of the pulmonary valve were obtained by segmenting phase contrast images with the same software. We estimated pulmonary regurgitation fraction (RF) by flow data. The pressure gradient (PG) was estimated from peak flow velocities using Bernoulli's equation as described.

Statistical analysis

Friedman test was used to compare EDVI, ESVI, SVI, EF, RF and PG before and after 1, 3, 6, 12, 24, 36, and 48 months from PPVI. All testing was performed using SPSS statistical software for Windows, release 14.0 (SPSS Inc., Chicago, IL, USA). *P* values lower than 0.05 were considered as significant.

Results

Overall, PG (31±06 to 16±4 mmHg), RF (16 ±17 to 0.3±1 %) significantly declined (p<0.001). A significant reduction of RV volumes (EDVI from 82±38 to 58±12 ml/m^2, p<0.001; ESVI from 44±12 to 30±13 ml/m^2, p<0.001), as well as a significant increase of RVEF (from 49±13 to 58±12%, p<0.001) and SVI (from 38±14 to 40±8 ml/m^2, p<0.001) was observed; RF and PG were significantly reduced at last follow-up (p<0.001). LV analysis showed a significant increase in EDVI (from 67±17 to 73±18 ml/m^2, p=0.034) and SVI (from 37±11 to 43±10 ml/m^2, p<0.001) while no significant changes were observed for ESVI and EF. One patient performed CMR with intracardiac defibrillator with the housing implanted on the right anterior side of the chest (Figure 4). Before CMR examinations, a dedicated cardiologist deactivated the device to avoid a wrong response during the examination.

Fig. 4

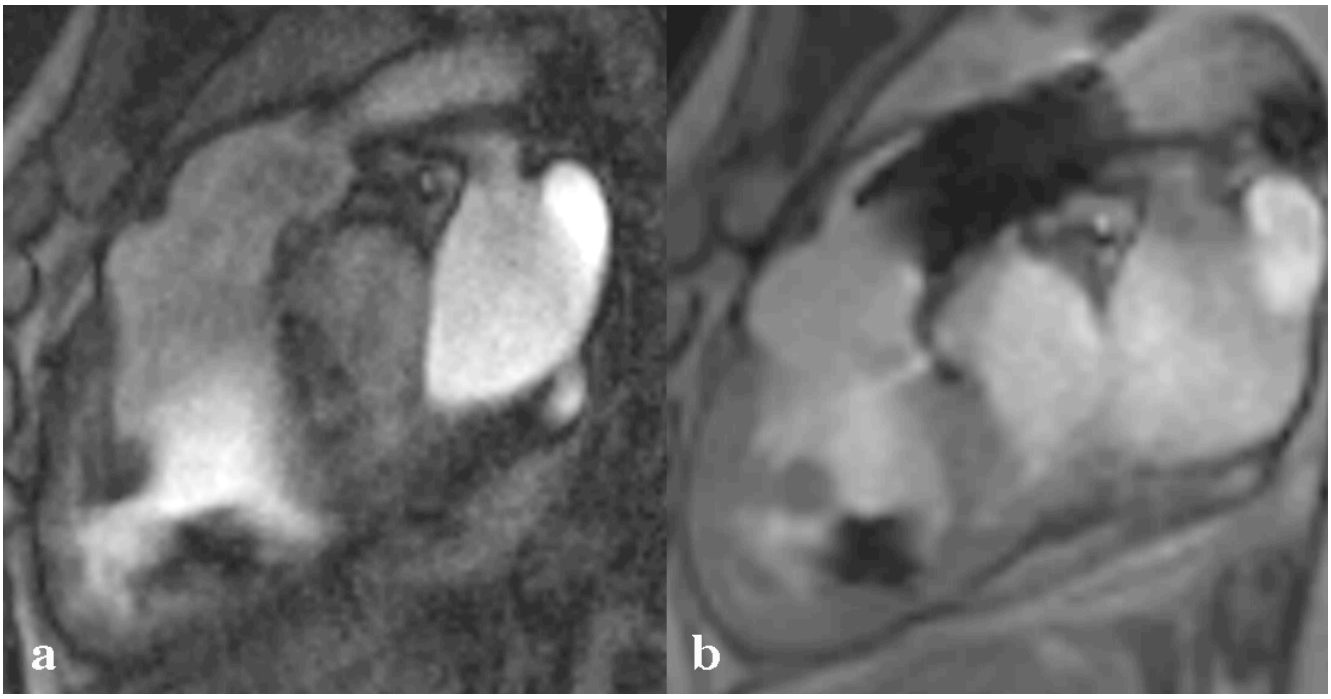

Two patients needed a surgical replacement of conduit after 24 and 36 months from PPVI respectively, due to a fracture of pulmonary stents. One patient needed a second implantation of a stent in pulmonary conduit after 24 months of PPVI due to a restenosis of the valve. We did not find any CMR sign or parameter that could predict the adverse events.

Discussion

In the last decade PPVI has emerged as the preferred treatment in pulmonary conduit dysfunction in CHD patients, being less invasive than surgical repair. We investigate with CMR a consecutive series of patients before and after PPVI to evaluate the immediate and mid-term changes in cardiac function values. We observed a significant and progressive reduction of RV volumes as well as a significant increase of RVEF and RVSVI during the investigated follow-up. The most important remodeling occurred by 3 months from PPVI. However, it was important to show what happened during following four years, when a further progressive remodeling was observed with a continuous increase of RVEF. Regarding flow analysis, both RF and PG were strongly reduced immediately (at 1 month follow-up) and thereafter stable at lowered values. These results were in agreement with literature [53, 54, 55], showing a good effect of PPVI on the RV function. However, to our knowledge, there are no studies showing

the follow-up of these patients up to 4 years after PPVI.

Interestingly, follow-up of LV volumes showed a significant increase in EDVI and SVI. The former result can be explained considering that the reduction of RVEDVI allows for a better diastolic compliance of LV, in turn determining an increased LVSVI. The improvement of LVEDVI likely reflects a decrease in RV volume and pressure overload, and hence reduction in consequent interventricular dependence from paradoxical septal motion. Conversely, the LVEF remained unchanged due to the not significant increase in LVESVI. Of note, one patient with an intracardiac defibrillator was fully studied with CMR with a comprehensive evaluation of RV and RV outflow tract function. The reason for this good result is that the housing of the device was implantated on the right side of the chest, causing artifacts not influencing heart imaging. This CMR was performed because the patient has been enrolled in an IRB-approved prospective study aimed at evaluating the MRI safety in patients having pacemakers or intracardiac defibrillators. PPVI implies some possible complications as stent fracture [35] or endocarditis [36]. In our population, two patients had stent fracture and one had endocarditis and stent restenosis. In the two cases of stent fracture a surgical implantation of a conduit was performed; in the case of restenosis a new stent was implanted. We did not find any CMR sign or parameter that could predict the adverse events, being the baseline and follow-up results not different from those patients who did not have any adverse events. Thus, while endocarditis is the most probable cause of restenosis, the only possible explanation for the fracture is a suboptimal correspondence between the stent geometry and the individual outflow tract anatomy. This study had some limitations. First, we retrospectively evaluated a heterogeneous sample of patients with congenital heart diseases originally treated with different surgical procedures. However, the series of patients was consecutive and all patients presented the same condition of pulmonary stenosis/insufficiency treated with PPVI. Second, we did not estimate the inter- and intra-observer reproducibility of CMR data. However, CMR is

widely considered more reproducible than echocardiography in the evaluation of the right chambers and pulmonary artery in a multiplanar and comprehensive evaluation [36]. Finally, only one type of pulmonary valve stent as described in Methods, so that our conclusion cannot be applied to other pulmonary valve stents.

In conclusion, a CMR four-year follow-up after PPVI demonstrated restored pulmonary conduit function, reduced RV volumes and increased RV and LV function. However, it did not predicted valve fracture/restenosis.

3.5. Semi-Automated Blood-threshold CMR Volume Analysis of Functional Univentricular Heart (Under revision)

Purpose

To validate a semi-automated blood-threshold (BT) segmentation software of cardiac magnetic resonance (CMR) cine images in patients with functional univentricular heart (FUH).

Materials and methods

Study population

The Ethics Committee approval was obtained for this retrospective study. A total of 70 CMR exams of patients with FUC performed at our institution between March 2008 and March 2015 were considered. The inclusion criteria for the re-assessment of the images were: 1) complete acquisition of cardiac volume with cine images and 2) acquisition of through-plane images of flow ascending aorta. Therefore, 15 exams were excluded, for a total of 55 exams remaining, obtained from 44 patients (7 patients were scanned 2 times, 2 patients 3 times). In case of repeated exam in the same patients, the time interval was at least 12 month. They were 30 males and 14 females with a mean age at the first examination of 25 years ±8 standard deviation. The youngest patient was 7 years old at the time of the examination, the oldest patient was 41 years old.

Image acquisition

All CMR examinations were performed with a 1.5-T unit (Magnetom Sonata Maestro Class or Magnetom AERA, Siemens Medical Solutions) with 40-mT/m or 35-mT/m gradient power respectively, using a four- or twelve channel surface phased-array coil placed over the thorax and with the patient in supine position. The image acquisition was gated to the ECG signal and respiration control (breath-holding) to produce a cine sequence throughout all the systole and diastole and to avoid cardiac and respiratory artifacts. A CMR study included a complete set of

short-axis (from base to apex) cine images, using an ECG-triggered steady-state free precession pulse sequence acquired with the following technical parameters: TR/TE 4.0/1.5 ms; FA 80°; slice thickness 8 mm; time resolution 45 ms; mean acquisition time 14±4 s. The phase contrast (PC) through-plane sequences were used for blood flow quantification. Images perpendicular to the ascending aorta were obtained. A breath-hold turbo spoiled gradient echo sequence (fast low-angle shot) was performed for phase-velocity mapping with the following technical parameters: TR/TE 4.0/3.2 ms; slice thickness 5 mm; velocity encoding (VENC) from 150 ms to 350 ms; time resolution 41 ms; mean acquisition time 15±4 s. Initially, we acquired the PC sequence with a VENC of 150 ms. In the presence of aliasing, we modified the VENC adding 50 ms for each new sequence, step-by-step up to the complete disappearance of the aliasing artifact. Flow measurements were performed right above the aortic valve. The PC through-plane sequences produced two sets of images: the magnitude image and the phase velocity map. The magnitude image provides details on the anatomy and identifies the boundaries of the vessel, while the phase velocity map corresponds to blood velocity [39].

Image assessment

Two independent readers with comparable experience (2 years) performed the segmentation of cardiac and flow images using MEDIS QMass 7.6 and QFlow 5.6 (Medis medical imaging systems, Leiden, The Netherlands. For the segmentation of cardiac images, in each session both readers independently manually traced the epicardial contour of the FUH both in the end-diastolic and end-systolic phases. Then the software applied the blood threshold technique (Mass-K mode) and calculated the end-diastolic volume (EDV), end-systolic volume (ESV), SV, ejection fraction (EF) and cardiac mass values in a totally automated way. For the segmentation of flow images of the ascending aorta, in each session the reader positioned a region of interest on the vessel boundary of a selected slice. Subsequently, the reader propagated the segmentation through the remaining slices and the software proposed an

automated adjustment and the reader was allowed to manually correct the adjusted contours. For each session forward flow and backward flow measurements were obtained.

Statistical analysis

The Wilcoxon method and Spearman correlation were used respectively to compare and correlate the median value of SV and aortic forward flow. The Bland-Altman method was used to estimate the intra- and inter-reader reproducibility. The intra-reader reproducibility was performed only for R1 with at least a 10-day interval between the two sessions. The coefficient of repeatability (CoR) was calculated as 1.96*standard deviation of differences of the two datasets. Reproducibility was reported as complement to 100% of the ratio between the CoR and the mean. Bias (mean of the differences of the two datasets), and 95% limits of agreement (bias ± 2 SD) were plotted as well.

Results

The image analysis was feasible in all patients and no artifacts prevented from a correct segmentation. The time needed for segmentation of cine and PC images was 15±2 minutes per exam.

Fifty-five exams were analyzed. The median value of SV and aortic forward flow were 57.7 ml (47.9–75.6) and 57.4 ml (48.9–80.4) respectively. We found a not significant difference (P =0.123) but a significant correlation (r=0.789, P <0.001) between mean SV and aortic forward flow.

The mean difference between the SV values measured by R1 was 0.12 ml accompanied by a CoR of 8.10 ml, corresponding to an intra-reader reproducibility of 86%. The mean difference between the aortic forward flow values was -0.1 ml accompanied by a CoR of 2 ml, corresponding to a reproducibility of 96%.

The inter-reader analysis of SV showed a CoR of 8.63 ml over a mean difference of -1.9 ml, corresponding to an inter-reader reproducibility of 85%; the same data for the aortic forward

flow were 2.12 ml over a mean difference of 0.24 ml corresponding to and inter-reader reproducibility of 96%. An example of segmentation of cine-images with threshold technique is shown in Figure 5

Fig. 5

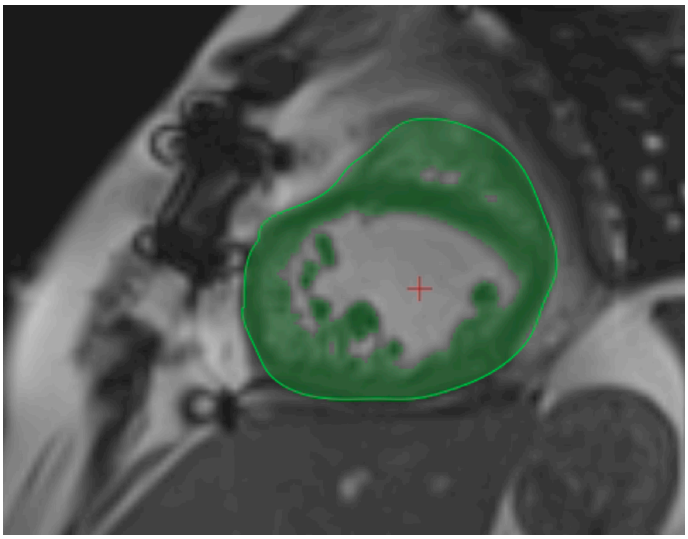

Discussion

Practical and theoretical advances in the treatment of FUH and in the clinical management of FC have greatly increased life expectancy of these patients. Physicians are now confronted, as in other forms of CHD, with a steady growing population of young and middle aged adults living on FC. This population requires a strict clinical follow-up to prevent or at least delay the onset of a large spectrum of complications, ultimately leading to a life-threatening failure of the FC and to the need of heart transplant [37]. The pivotal role of cardiac imaging in this rigorous strategy of follow-up has been widely demonstrated, and so have been the considerable advantages of CMR compared to other imaging techniques that could be used to perform a functional or anatomical evaluation of FC, namely echocardiography and computed tomography (CT) [38]. Constant advances in CMR techniques and equipment in the last decade grant now adequate anatomical detail in addition to the accurate and not operator-

dependent functional assessment of ventricular chambers (main and accessory), cardiac valves and intra or extra-cardiac shunts and conduits. Furthermore, the routine use of CMR in the imaging of FC not only does not usually require the intravenous administration of contrast mediums, but also conveniently restricts the use of CT and therefore patient's exposure to ionizing radiation to occasional circumstances that require a very highly detailed anatomical assessment of the FC [39]. Volume and function assessment is achieved through the segmentation of cine images. This post-processing technique, that in its first applications was exclusively manually performed by a trained reader, implies the recognition of the difference between the blood pool in the ventricular cavity, other anatomical structures normally in the ventricular chamber such as trabeculae and papillary muscles (TPM) and the ventricular walls. Manual tracing of contours for the ventricular walls and TPM by an experienced reader still constitutes the most widely validated and employed approach, but in the last decade several studies have validated semi-automated techniques that, while less time-efficient than a fully automated solution, try to address its numerous limitations and provide a solid method, well-balanced in terms of cost-effectiveness analysis, to obtain a proper estimate of ventricular volume and mass with minimal manual input [40]. One of these limitations is the correct allocation of TPM to the myocardial mass. TPM were shown to substantially influence the accuracy of ventricular volume and mass assessment, but the exclusion of TPM from the blood pool obtained with a painstaking manual tracing of endocardial contours results in a greatly increased length of the post-processing stage and presents an high intra- and inter-reader variability, resulting in a customary misattribution bias for TPM when the fully manual tracing of contours is employed [41–43] . A BT technique such as the Mass-K Mode algorithm can serve as a time-saving and accurate solution to this notable issue. In this technique, after the reader has manually traced only the epicardial contours on the end-systolic and end-diastolic phases of the cine-images, the software calculates a blood percentage for each pixel inside the

contoured area considering the different signal intensity of blood and myocardium. After visual inspection, the reader can freely alter, in any slice and phase, the default threshold value (50%) of signal intensity discrimination. Moreover, semi-automated detection of the epicardial margin can be used, requiring only small manual adjustments in good quality images and thus further curtailing the time required for the post-processing stage [43]. The Mass-K Mode algorithm has been validated for clinical routine application, showing both accurate and reproducible evaluation of ventricular mass and volume and reduced time of analysis, by Jaspers et al. [82] on phantoms and 12 patients with normal cardiac anatomy and function and more recently by Varga-Szemes et al. [40] on 137 patients with a broad range of cardiac diseases but not affected by CHD. The results of our study validate the use of this blood-threshold technique in patients with a thoroughly abnormal cardiac anatomy, such as the one that is found in patients with FC. In the absence of other reference tools to validate ventricular volume assessments, we choose to use aortic flow measurements as an independent benchmark for SV since previous studies showed it to be a solid and reproducible standard and we found no statistically significant difference and a significant correlation between the two value. Moreover, greater level of automation and lesser need of manual adjustments granted by the use of the blood threshold technique and the semi-automated recognition of epicardial contours and of aortic walls account for the excellent inter- and intra-reader reproducibility of both SV and aortic flow volume, respectively around 85% and 96%.

Our study has limitations: first, it is a retrospective study on a relatively small number of subjects and is based on a single-center historical series of FC patients; however FUV patients are a very small population and usually referred to a single center. Second, it is possible that, due to the retrospective structure of our study, even small differences in the acquisition parameters, reasonably likely to happen in the absence of standardized CMR acquisition protocol, may have negatively influenced the quality of cine-images and therefore the

performance of the BT technique. Third, the study lacks an independent reference standard, even though the aortic flow analysis may be considered substantially independent from the cardiac cine study.

To summarize, we successfully validated the use of a BT technique for the segmentation of cine-images in patients with FC. We observed a high intra- and inter-reader reproducibility for the assessment of ventricular stroke volume and excellent agreement with aortic flow values used as benchmark. In routine clinical and diagnostic practice, the shortening of post-processing and the accurate quantification of cardiac function may have a positive impact on the follow-up of patients with FC.

4. Conclusions

We contributed to show the possibility, using dedicated protocols, to obtain an impressively low ionizing dose reduction in CHD patients also using standard 64-slice CT scanners (paper 2.1). This really open a new windows of opportunities for using CCT in CHD, especially when CMR requires long sedation times and a high spatial resolution is considered useful for treatment planning.

Conversely, CMR holds a pivotal role when functional and flow imaging is required. We showed the role of CMR in evaluating of patients percutaneously implanted with a pulmonary valve (papers 3.1 and 3.4). Moreover, we proposed two new approaches for post-processing CMR images, regarding volume estimation of patients with a single ventricle, a rare CHD (papers 3.2 and 3.5) and a method for quantifying the paradoxical septal motion (paper 3.3), a typical consequence of alteration of right heart function that can happen in CHD.

In conclusion CMR and CCT are two fundamental imaging techniques to evaluate patients with complex CHD. In the last years, we are moving from a competition to cooperation between CCT and CMR. Both imaging modalities have limitations and advantages. CMR can evaluate heart function vessel flow but require a long acquisition time and in same patients a long sedation time. CCT has a very high spatial resolution and short acquisition time but implies ionizing radiation exposure. On the one side, we confirming the crucial role of CMR when function analysis is required but also showed the relevant possibilities of x-ray dose reduction in CCT, also using standard 64-slice scanners in the study of CHD patients.

5. References

1. Hoffman JI, Kaplan S. The incidence of congenital heart disease. J Am Coll Cardiol 2002;39:1890-1900
2. Roguin N, et al. High prevalence of muscular ventricular septal defect in neonates. J Am Coll Cardiol 1995;26:1545-1548.
3. Secchi F et al. MR imaging of aortic coarctation. Radiol Med 2009;114:524-537.
4. Yoo S et al. Magnetic resonance imaging of complex congenital heart disease. Int J Card Imaging 1999;15:151-160.
5. Cohen MS et al. Multimodality Imaging Guidelines of Patients with Transposition of the Great Arteries: A Report from the American Society of Echocardiography Developed in Collaboration with the Society for Cardiovascular Magnetic Resonance and the Society of Cardiovascular Computed Tomography. J Am Soc Echocardiogr. 2016 Jul;29(7):571-621
6. Hascoët S et al. Cardiac imaging of congenital heart diseases during interventional procedures continues to evolve: Pros and cons of the main techniques. Arch Cardiovasc Dis. 2016 Feb;109(2):128-42
7. Alfakih K et al. Assessment of ventricular function and mass by cardiac magnetic resonance imaging. Eur Radiol 2004;14:1813-1822.
8. Spevak, P.J et al Surgically corrected congenital heart disease: utility of 64-MDCT. AJR Am J Roentgenol, 2008. 191(3): p. 854-61.
9. Tricarico F et al. Cardiovascular CT angiography in neonates and children: Image quality and potential for radiation dose reduction with iterative image reconstruction techniques. Eur Radiol 2013;23:1306-15
10. Arnold R, Ley S, Ley-Zaporozhan J, et al. Visualization of coronary arteries in patients after childhood Kawasaki syndrome: Value of multidetector CT and MR imaging in comparison to conventional coronary catheterization. Pediatr Radiol 2007;37:998–1006.

11. Lee T, Tsai I-C, Fu Y-C, et al. Using multidetector-row CT in neonates with complex congenital heart disease to replace diagnostic cardiac catheterization for anatomical investigation: initial experiences in technical and clinical feasibility. Pediatr Radiol 2006;36:1273–82.
12. Han BK, Rigsby CK, Hlavacek A, et al. Computed Tomography Imaging in Patients with Congenital Heart Disease Part I: Rationale and Utility. An Expert Consensus Document of the Society of Cardiovascular Computed Tomography (SCCT): Endorsed by the Society of Pediatric Radiology (SPR) and the Nor. J Cardiovasc Comput Tomogr 2015;9:475–92.
13. Cademartiri F, Di Cesare E, Francone M, et al. Italian Registry of Cardiac Computed Tomography. Radiol Medica 2015;120:919–929.
14. Nordmeyer J, Gaudin R, Tann OR, et al. MRI may be sufficient for noninvasive assessment of great vessel stents: an in vitro comparison of MRI, CT, and conventional angiography. AJR Am J Roentgenol 2010;195:865-871
15. McElhinney DB, Hellenbrand WE, Zahn EM, et al. Short- and medium-term outcomes after transcatheter pulmonary valve placement in the expanded multicenter US melody valve trial. Circulation 2010; 122:507-516
16. Eicken A, Ewert P, Hager A, et al. Percutaneous pulmonary valve implantation: two-centre experience with more than 100 patients. Eur Heart J 2011;32:1260-1265
17. Lurz P, Nordmeyer J, Giardini A, et al. Early versus late functional outcome after successful percutaneous pulmonary valve implantation: are the acute effects of altered right ventricular loading all we can expect? J Am Coll Cardiol 2011;57:724-731
18. Romeih S, Kroft LJ, Bokenkamp R, et al. Delayed improvement of right ventricular diastolic function and regression of right ventricular mass after percutaneous pulmonary valve implantation in patients with congenital heart disease. Am Heart J 2006;158:40-46
19. Capelastegui Alber A, Astigarraga Aguirre E, de Paz MA, et al. Study of the right ventricle using magnetic resonance imaging. Radiologia 2011;54:231-245

20. Kilner PJ. The role of cardiovascular magnetic resonance in adults with congenital heart disease. Progress in Cardiovascular Dis 2011;295–304
21. Broberg CS , Meadows A , Sahn D. Magnetic resonance imaging images in adult congenital heart disease. Curr Probl Cardiol 2011;36:228-255
22. Deanfield J, Thaulow E, Warnes C, et al. Management of grown up congenital heart disease. Eur Heart J 2003;24:1035-1084
23. Parra DA, Vera K. New imaging modalities to assess cardiac function: not just pretty pictures. Curr Opin Pediatr 2012;24:557-564
24. Pennell DJ. Ventricular volume and mass by CMR. J Cardiovasc Magn Reson 2012;4:507-513
25. Geva T, Powell AJ, Crawford EC et al. Evaluation of regional differences in right ventricular systolic function by acoustic quantification echocardiography and cine magnetic resonance imaging. Circulation 1998;98:339-45
26. Bodhey NK, Beerbaum P, Sarikouch S et al. Functional analysis of the components of the right ventricle in the setting of tetralogy of Fallot. Circ Cardiovasc Imaging 2008;1:141-7
27. Soriano BD, Hoch M, Ithuralde A, et al. Matrix-array 3-dimensional echocardiographic assessment of volumes, mass, and ejection fraction in young pediatric patients with a functional single ventricle: a comparison study with cardiac magnetic resonance. Circulation 2008;117:1842-1848
28. Kardesoglu E, Cebeci BS, Celik T, et al. Assessment of interventricular septal motion using colour tissue Doppler imaging in adult patients with atrial septal defect. J Int Med Res 2004;32:14−18.
29. Giubbini R, Rossini P, Bertagna F, et al. Value of gated SPECT in the analysis of regional wall motion of the interventricular septum after coronary artery bypass grafting. Eur J Nucl Med Mol Imaging 2004;31:1371−1377.

30. Sibille L, Bouallegue FB, Bourdon A, et al. Comparative values of gated blood-pool SPECT and CMR for ejection fraction and volume estimation. Nucl Med Commun 2011:32:121–128.
31. Muzzarelli S, Ordovas KG, Cannavale G, et al. Tetralogy of Fallot: impact of the excursion of the interventricular septum on left ventricular systolic function and fibrosis after surgical repair. Radiology 2011;259:375–383.
32. Roeleveld RJ, Marcus JT, Faes TJ, et al. Interventricular septal configuration at mr imaging and pulmonary arterial pressure in pulmonary hypertension. Radiology 2005;234:710–717.
33. Louie EK, Bieniarz T, Moore AM, et al. Reduced atrial contribution to left ventricular filling in patients with severe tricuspid regurgitation after tricuspid valvulectomy: a Doppler echocardiographic study. J Am Coll Cardiol 1990;16:1617-1624.
34. Mori S, Nakatani S, Kanzaki H, et al. Patterns of the interventricular septal motion can predict conditions of patients with pulmonary hypertension. J Am Soc Echocardiogr 2008;21:386–393.
35. Butera G, Milanesi O, Spadoni I et al. Melody transcatheter pulmonary valve implantation. Results from the registry of the Italian Society of Pediatric Cardiology. Catheter Cardiovasc Interv 2013;81:310-6
36. Caudron J Fares J Lefebvre V Vivier PH Petitjean C Dacher JN. Cardiac MRI assessment of right ventricular function in acquired heart disease: factors of variability. Acad Radiol. 2012 Aug;19(8):991-1002.
37. d'Udekem Y, Iyengar AJ, Cochrane AD, Grigg LE, Ramsay JM, Wheaton GR, et al. The Fontan Procedure: Contemporary Techniques Have Improved Long-Term Outcomes. Circulation. 2007;116:I157-I-164.
38. Margossian R, Schwartz ML, Prakash A, Wruck L, Colan SD, Atz AM, et al. Comparison of Echocardiographic and Cardiac Magnetic Resonance Imaging Measurements of

Functional Single Ventricular Volumes, Mass, and Ejection Fraction (from the Pediatric Heart Network Fontan Cross-Sectional Study). Am. J. Cardiol. Elsevier Inc.; 2009;104:419–28.

39. Walsh M a., Noga M, Rutledge J. Cumulative Radiation Exposure in Pediatric Patients with Congenital Heart Disease. Pediatr. Cardiol. 2015;36:289–94.
40. Varga-Szemes A, Muscogiuri G, Schoepf UJ, Wichmann JL, Suranyi P, De Cecco CN, et al. Clinical feasibility of a myocardial signal intensity threshold-based semi-automated cardiac magnetic resonance segmentation method. Eur. Radiol. 2015; 26:1503-11.
41. Chuang ML, Gona P, Hautvast GLTF, Salton CJ, Blease SJ, Yeon SB, et al. Correlation of trabeculae and papillary muscles with clinical and cardiac characteristics and impact on CMR measures of LV anatomy and function. JACC Cardiovasc. Imaging. Elsevier Inc.; 2012;5:1115–23.
42. Weinsaft JW, Cham MD, Janik M, Min JK, Henschke CI, Yankelevitz DF, et al. Left ventricular papillary muscles and trabeculae are significant determinants of cardiac MRI volumetric measurements: Effects on clinical standards in patients with advanced systolic dysfunction. Int. J. Cardiol. 2008;126:359–65.
43. Papavassiliu T, Kühl HP, Schröder M, Süselbeck T, Bondarenko O, Böhm CK, et al. Effect of endocardial trabeculae on left ventricular measurements and measurement reproducibility at cardiovascular MR imaging. Radiology. 2005;236:57–64.